# Autoionizing Rydberg states of NO in strong electric fields

J. B. M. Warntjes
*FOM-Institute for Atomic and Molecular Physics (AMOLF), Kruislaan 407, 1098 SJ Amsterdam, The Netherlands*

F. Robicheaux
*FOM-Institute for Atomic and Molecular Physics (AMOLF), Kruislaan 407, 1098 SJ Amsterdam, The Netherlands and Department of Physics, Auburn University, Auburn, Alabama 36849*

J. M. Bakker, and L. D. Noordam
*FOM-Institute for Atomic and Molecular Physics (AMOLF), Kruislaan 407, 1098 SJ Amsterdam, The Netherlands*

(Received 24 March 1999; accepted 29 April 1999)

We report on an investigation on autoionization of Rydberg electrons of the nitric oxide molecule in strong, static electric fields. The excitation was done via various rotational states of the $A\,^2\Sigma^+$ intermediate state ($v'=0$) and with polarization parallel or perpendicular to the electric field. The splitting of the autoionizing Rydberg states into overlapping Stark manifolds is resolved for excitation above the saddlepoint created by the field. We observe that the competing decay between photoionization and predissociation can lead to an incorrect interpretation of threshold energy. The photoionization spectrum of NO Rydberg series attached to various rotational thresholds is very similar owing to weak rotational coupling. The experimental results are accurately simulated by quantum calculations based on multichannel quantum defect theory (MQDT). A more intuitive formulation of the average behavior of the photoionization cross section is developed that accounts for the suppression of ionization near the threshold due to competing predissociating channels.  [S0021-9606(99)01128-9]

## I. INTRODUCTION

An optical pulse can pump the outer electron of an atom or molecule toward quantized, highly excited states, so-called Rydberg states, with energies described by the Rydberg formula $E=\mathrm{IP}-1/2(n-\mu)^2$ (in atomic units), where IP is the ionization potential, $n$ is the principle quantum number ranging from one to infinity, and $\mu$ is the quantum defect.[1] The classical outer turning point of the electron orbit of such a Rydberg state is rather large (for instance 660 Å for $n=25, l=0$; 800 times the internuclear distance of the diatomic molecule NO), and the time it takes to complete the orbit is relatively long (2.4 ps for $n=25$; the same time scale as the lowest rotations of the NO core). Upon applying a static electric field to the system, the Rydberg levels experience a Stark splitting and the angular momentum of the orbiting electron is no longer conserved. Hence, in addition to the oscillation along the radial coordinate, there is also an oscillation in the angular momentum of the electron between $l=0$ up to $l=n-1$ and back. For $n=25$ with a field strength of 1 kV/cm, the angular momentum period is 10.4 ps. In that case, the electron makes about four radial oscillations during one complete angular oscillation.

A simultaneous effect of the electric field is a suppression, in the direction of the field, of the Coulomb potential experienced by the outer electron. In this direction the electron can escape over the created saddlepoint with a lower energy than in zero-field. In fact, at a field strength of 1 kV/cm the potential is suppressed so much that the $n=25$ Rydberg level, in zero-field bound by 176 $\mathrm{cm}^{-1}$, can classically escape over the saddlepoint (field-induced autoionization). For the NO molecule the time scale on which this electron emission process takes place is on the same order as fragmentation of the core (predissociation). Each time an electron returns to the ionic core there is a probability that it scatters and autoionizes and there is a probability that the energy of the electron is transferred back to the core, leading to fragmentation into a neutral nitrogen and oxide atom.

In addition to autoionization and predissociation, coupling of the electron to the molecular core can lead to an exchange of core rotational or vibrational energy to the electron. We refer to the case that the Rydberg electron gains rotational or vibrational energy sufficient to escape the ionic core as rotational or vibrational autoionization, respectively.

In order to unravel the influence of the various decay mechanisms of Rydberg electrons in a static electric field, we monitor the photoionization of NO at various field strengths. Nitric oxide has been selected as an example to study these dynamics, since the molecule has a convenient and established laser excitation scheme. The excitation pathway is schematically depicted in Fig. 1. The molecule is excited from the $^2\Pi$ ground state via a selected rotational state of the $A\,^2\Sigma^+$ intermediate state ($v'=0$) to the Rydberg series. A static electric field is present that lowers the potential energy of the Rydberg electron in the direction of the field. The photoionization yield is monitored as a function of excitation frequency of the second laser step.

 

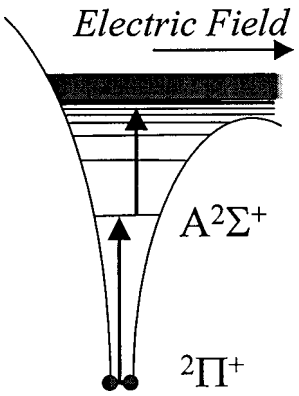


FIG. 1. Schematic excitation scheme of nitric oxide in a static electric field. The molecule is excited with $1+1'$ REMPI from the $^2\Pi$ ground state via the $A\,^2\Sigma^+$ intermediate state to the Rydberg series. The static electric field lowers the potential energy of the Rydberg electron on one side.

## II. THEORY

In this section we will describe the full MQDT calculations that give excellent agreement with the observed spectra. However, we will begin with the physical mechanisms starting from a hydrogen atom in a static electric field.

### A. Influence of a static electric field

A static electric field has various effects on a molecule. As mentioned already, it creates a suppression of the Coulomb potential of the molecular core in the direction of the field. The potential energy of the Rydberg electron, when far from the core, can be described as the sum of the Coulomb potential and the potential created by the field strength $F$ pointing in the direction $z$,

$$E=\frac{-1}{|r|}-Fz. \tag{1}$$

The Coulomb potential is raised on one side and lowered on the other by the electric field. The energy of the local maximum on the lowered side (the saddlepoint) as a function of field strength $F$ is then

$$E=-\alpha\sqrt{F}, \tag{2}$$

with $\alpha=2$ in atomic units, or $\alpha=6.12\,\mathrm{cm}^{-1}$ if the field is given in V/cm.

In a typical photoionization measurement the photoelectron yield is detected as a function of excitation energy. One would expect a signal with a stepfunction-like appearance: no signal below the saddlepoint and electron autoionization yield from the quantized states above the saddlepoint. The threshold can, in a series of such measurements, be tracked as a function of field strength yielding the experimental value of $\alpha$.

Another effect of a static electric field $F$ is that it breaks the conservation of angular momentum of the Rydberg electron or, equivalently, the $n$-fold degeneracy of a Rydberg state $n$ is lifted and splits into a Stark manifold of $n$ separate $k$-states. The energy of the Rydberg Stark states to lowest order in the field strength $F$ is

$$E=\frac{-1}{2n^2}+\frac{3}{2}Fnk, \tag{3}$$

where the quantum number $k$ runs from $(n-1,n-3...-n+1)$ for the azimuthal angular momentum $m=0$. The states that increase in energy compared to the zero-field value (positive $k$) are called blue states; those that decrease in energy (negative $k$) are called red states. Note that above the saddlepoint energy the manifolds of adjacent $n$ always overlap because the spread in energy of the manifolds is so large.

So far these considerations are general for atoms and molecules. Molecules have internal degrees of freedom, and each of these rotations and vibrations has its own Rydberg series, hence we have to consider a far larger number of states than for atoms. The rotational series are separated by the rotational energy $E_{\mathrm{rot}}$, which is given in first order for Hunds case b (intermediate $\Sigma$ state) and case d (Rydberg state) by

$$E_{\mathrm{rot}}=BN(N+1), \tag{4}$$

with $B$ the rotational constant and $N$ the rotational angular momentum of the molecular core (note: we use $N'$ for the $A\,^2\Sigma^+$ state and $N^+$ for the ionic state). Throughout these experiments, we excite Rydberg series attached to the lowest rotational states of the zeroth vibration of NO. In a static electric field where every Rydberg level splits up into $n$ $k$-states, the system is more prone to accidental degeneracy of states of different rotation, leading to an enhanced coupling of several rotational series. These arguments are well known from zero kinetic energy (ZEKE) spectroscopy.[2] Series that couple to continuum states, either directly, or via lower rotational series, induce rotational autoionization.[3–6]

The Rydberg series in NO and their lifetimes and couplings are quite well known.[7–13] Also other decay channels like predissociation are reported.[7,8,14–16] However, important features of Rydberg electrons in a strong electric field have received little attention.

### B. Quantum calculation of the photoionization spectra

We have based our simulations of the photoionization spectra of NO in a static field on the multichannel Stark theory.[17] This formulation uses the Wentzel–Kramers–Brillouin (WKB) treatment of the Stark problem to describe alkali atoms in static electric fields,[18] in order to include the possible exchange of energy and angular momentum between the Rydberg electron and the molecular ion core. Our formalism is very similar in spirit to the treatment presented in Ref. 19, but also allows the calculation of the partial excitation amplitudes into all of the channels, enabling us to distinguish between the photoionization and photodissociation channels in our calculation.

The treatment in Ref. 17 uses a separation of quantum numbers into those appropriate in zero-field and those appropriate in an electric field. The reason for this separation is that when the Rydberg electron is near the ion (within 10–20 Bohr radii) the static field plays no role compared to the electron–ion interaction. Within this small volume, compli-

cated molecular processes can occur (coupling between different rotational and vibrational channels and between Rydberg channels and predissociation channels), but these processes are completely unaffected by the field. Thus, field-free channel couplings (parameterized by *K*-matrices) and dipole matrix elements can be used to describe the small *r* behavior of the Rydberg electron. When the electron is farther out than 10–20 Bohr radii from the ion, the potential is nearly identical to that of a H atom in a static field. We neglected any long-range interactions. In this outer region, the electron moves in uncoupled channels in parabolic coordinates. It is the connection between these two regions that gives the full wave function and allows us to obtain the full multichannel wave function in the field.

Another, more practical, reason for the separation of quantum numbers is that the formulation distinguishes between the channels which have nonzero scattering and those which have roughly zero scattering in zero field. Since the channels that do not have scattering (i.e., quantum defects that are effectively zero) behave like H, we can account for them implicitly without the need for including them in our matrix manipulations. This substantially improves the efficiency of the calculation, which is important because it is necessary to calculate the cross sections at 16 000 to 32 000 different energies for many different field strengths and initial states.

We will sketch the series of transformations that connect the wave function across different regions of space where different physical processes dominate. Let the parameter $\gamma$ indicate all of the zero-field channels that have nonzero *K*-matrix elements (i.e., these are the channels for which the Rydberg electron experiences non-Coulombic potential). In general, $\gamma$ describes five quantum numbers, and for this molecular situation,

$$\gamma=\{v,N^+,M_N,l,m\}, \tag{5}$$

where $v$ is the vibrational state of NO which is 0 for the cases we investigated, $N^+,M_N$ are the total and *z*-component of all nuclear angular momenta, and *l,m* are the orbital angular momentum and the *z*-component of the orbital angular momentum for the Rydberg electron. Note there is no coupling between states for which $M_N+m=M_{\mathrm{tot}}$ changes.

The quantum numbers in the field have a form similar to those in zero field. We define the parameter $\mathbb{N}$ to be the quantum numbers in parabolic coordinates,

$$\mathbb{N}=\{v,N^+,M_N,n_1,m\}, \tag{6}$$

which are similar to the $\gamma$ quantum numbers but with the angular momentum of the Rydberg electron replaced with the quantum number in the electric field, $n_1$, which is the number of nodes in the up-potential parabolic coordinate.

The formulation of Ref. 17 is general in the sense that it applies equally well to atoms or molecules in an electric field. The field dependent transformation between spherical and parabolic coordinates and the field dependent phases are independent of the short-range interactions between the atomic or molecular ion and the Rydberg electron. The only input into the Stark calculations that distinguishes between different ions are three kinds of body frame parameters: the zero-field threshold energies, the zero-field *K*-matrices in the $\gamma$ quantum numbers, and the zero-field dipole matrix elements in the $\gamma$ quantum numbers. In Table I are the last two body frame parameters we used in the calculation. For single channels, the *K*-matrices are $\tan(\pi\mu)$ with the quantum defects $\mu$ taken from Ref. 8. The $l=0,\Lambda=0$ and $l=2,\Lambda=0$ channels are coupled in the body frame; for these two channels, the *K*-matrix is given as $K_{ss}$ and $K_{sd}$ in the first row and $K_{ds}$ and $K_{dd}$ in the second row. To obtain the lab frame parameters, we use the frame transformation applied to molecular rotations.[20,21]

TABLE I. Body frame parameters for NO. $l$ is the orbital angular momentum of the Rydberg electron, $\Lambda$ is the projection of the angular momentum on the internuclear axis, $K$ are the $K$-matrix elements, and $D$ are the dipole matrix elements. The $l=0,\Lambda=0$ and $l=2,\Lambda=0$ channels are coupled in the body frame and the $K$-matrix is given as $K_{ss}$ and $K_{sd}$ in the first row and $K_{ds}$ and $K_{dd}$ in the second row.

| $l$ | $\Lambda$ | $K$ | $K$ | $D$ |
|---|---|---|---|---|
| 0 | 0 | 0.395 | −0.459 | 0.0 |
| 2 | 0 | −0.459 | 0.223 | 0.0 |
| 1 | 0 | −1.342 | | 1.3 |
| 1 | 1 | −1.058 | | 1.0 |
| 2 | 1 | −0.168 | | 0.0 |
| 2 | 2 | 0.287 | | 0.0 |

The frame transformation from the body frame to the (zero-field) lab frame is not sufficient to obtain quantum numbers in the form $\gamma$ of Eq. (5). The transformation gives the channel couplings in terms of the quantum numbers $\{v,N^+,l,J,M\}$, where $J$ is the total angular momentum and $M$ its *z*-component. We need to separate the total angular momentum $J$ into the nuclear rotational angular momentum and the angular momentum of the Rydberg electron. This is accomplished through one last recoupling that uncouples the $N^+$ and $l$ angular momenta. The unitary matrix that performs this recoupling is simply a Clebsch–Gordon coefficient,

$$\langle JM|M_N,m\rangle=\langle N^+M_N lm|N^+lJM\rangle. \tag{7}$$

After this sequence of recouplings, the *K*-matrices and dipole matrix elements have the correct form.

There is one last important ingredient that still needs to be incorporated. This is the possibility that the electron can be converted from its nearly free Rydberg character into a tightly bound electron in a predissociating orbital. Thus each time the electron returns to the region near the nucleus there is an $l$ dependent probability that it will be captured and disappear in a predissociating channel. We include this effect by extending the zero-field *K*-matrix so that each channel is coupled to an open channel with a strength that reproduces the zero-field predissociation rate. The electric field does not affect these extra channels so they are treated as completely open in our formulation. This channel provides extra width to each resonance and causes a reduction of the photoionization cross section since the predissociation is another pathway for decay.

### C. Average behavior of the photoionization cross section

To focus on the overall, average shape of the photoionization spectrum, including the dramatic effect of predissociation, we assume that the Stark spacing between Rydberg states of one manifold is not resolved. The basic idea is that by averaging over the Stark spacing almost all of the quantum standing wave behavior is lost. Therefore, the amount of flux into the ionization channel or detachment channel can be found by investigating how much each partial wave scatters into each channel. This works because on average the partial waves are equally populated over the energy range and they each scatter independently; for some Stark resonance states, the partial waves scatter constructively, but for other states they scatter destructively so that on average they behave as if they scatter independently. The average photoionization cross sections, modified due to the competing mechanism of predissociation, can give accurate information about dissociation rates of Rydberg states.

We will treat the simplest situation in detail; the extension to more complex situations is straightforward. The probability for direct electron ejection down potential depends on the function

$$\Phi_{lm}(\cos\theta_s)=2\pi\int_{-1}^{\cos\theta_s}|Y_{lm}|^2 d\cos\theta, \tag{8}$$

where $\theta_s$ is the maximum escape angle of the electron with respect to the direction of the field (the $-1$ direction), $l$ is the angular momentum of the Rydberg electron, and $m$ its projection on the field axis. We assume that the initial excitation to the Rydberg state is mainly into one partial angular momentum wave, $l_0$. The probability for the direct ejection of the electron from the molecule is

$$\eta=\Phi_{l_0 m}(\cos\theta_s). \tag{9}$$

The remaining fraction $1-\eta$ is bound but can still ionize by scattering of the molecular core. We define the branching ratio for ionization, $B_{\rm ion}$, as the probability for the bound electron to elastically scatter into the open region of space, $S_i$, divided by the sum of the probabilities to elastically scatter into the open region $S_i$ and to scatter into dissociation, $S_d$,

$$B_{\rm ion}=\sum_{l=|m|}S_i(l)\Big/\sum_{l=|m|}[S_i(l)+S_d(l)]. \tag{10}$$

We assume that the electric field thoroughly mixes the $l$'s so that all of them are equally likely. For the $l$ partial wave, the probability to scatter and leave the molecule is

$$S_i(l)=4\Phi_{lm}(\cos\theta_s)\sin^2(\pi\mu_l), \tag{11}$$

where $\mu_l$ is the quantum defect, and the probability to dissociate is

$$S_d(nl)=2\pi\Gamma_0(l)=2\pi(n-\mu_l)^3\Gamma_{\rm dis}(nl), \tag{12}$$

where $2\pi(n-\mu_l)^3$ is the Rydberg period in atomic units and $\Gamma_{\rm dis}(nl)$ is the zero-field dissociation rate of the $nl$ state in atomic units.

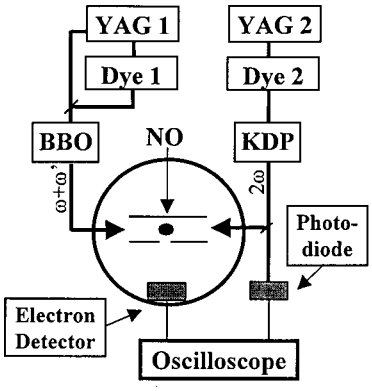


FIG. 2. Schematic overview of the experimental setup. The output of the Nd:YAG-pumped dye laser 1 is mixed with the third harmonic of the Nd:YAG laser in a BBO crystal. The resulting UV pulse (wavelength region 225–227 nm) excites the outer electron of NO from the ground state to a specific rotational level the $A\,^2\Sigma^+$ intermediate state ($v'=0$). The output of the Nd:YAG-pumped dye laser 2 is frequency doubled in a KDP crystal (wavelength region 320–330 nm) which excites the electron to Rydberg states. The interaction region of the NO beam and the laser pulses lies between two plates with a homogeneous static electric field. The total electron yield is detected by an electron detector and oscilloscope. Simultaneously the laser intensity is monitored by a photodiode.

Finally we define $D_i$ to be the direct excitation amplitude into the electron excitation channel. The energy averaged ionization cross section in terms of these parameters is

$$\sigma_{\rm ion}^F\propto|D_i|^2(\eta+[1-\eta]B_{\rm ion}). \tag{13}$$

We define $D_d$ as the direct excitation amplitude into the molecular dissociation channel and the energy averaged dissociation cross section is

$$\sigma_{\rm dis}^F\propto|D_d|^2+|D_i|^2(1-\eta)(1-B_{\rm ion}). \tag{14}$$

There are two points to notice about these cross sections. The first is that the sum of the ionization and dissociation cross sections in the field equals the sum of the two cross sections in zero field. The second is that the ionization cross section goes to zero in a smooth manner as $E$ decreases to $-2\sqrt{F}$; the exact manner in which it decreases to zero depends on how well the electron can elastically scatter down potential compared to how well it can cause dissociation.

## III. EXPERIMENTAL SETUP

For nitric oxide, the $n=25$ manifold of the Rydberg series converging to the lowest rovibrational state has an energy around 74 546 $\rm cm^{-1}$ above the ground state (lowest ionization potential is 74 721.7 $\rm cm^{-1}$,[22]) which we can, in principle, reach with one photon of 134 nm. However, since we start at a finite temperature there is a rotational and vibrational ground-state population distribution, which can all be excited by that wavelength. The result of excitation will be a whole distribution of excited Rydberg levels on many rotational states close to the ionization potential. Consequently, we employed the following $1+1'$ photon excitation scheme. First we excite from the ground state to an intermediate $A\,^2\Sigma^+$ state ($v'=0$) with a narrow-band ultraviolet (uv) pulse in the region 225–227 nm. The rotational structure of the $A\,^2\Sigma^+$ state is well known.[23–25] The wavelength

of the first laser pulse is set to populate a specific rotation of the zeroth vibration of the molecular core. From there on we excite with another narrow-band pulse in the region 320–330 nm toward the Rydberg states. In this way we populate Rydberg states from only one initial rotation and vibration.

The experiments were performed with the setup schematically depicted in Fig. 2. A supersonic jet expansion of pure nitric oxide gas was used from a pulsed valve with a backing pressure of one atmosphere into the vacuum chamber with a typical background pressure of $10^{-6}-10^{-5}$ mbar. The pulsed valve is placed 4 cm from the interaction region, where the two UV pulses with a delay of 5 ns excite the molecules from their ground state to the Rydberg series. For the excitation step from the NO $^2\Pi$ ground state toward the $A\,^2\Sigma^+$ intermediate state ($v'=0$), the output of a 10 Hz Nd:YAG laser pumped dye (1) laser (tunable in the range 615–630 nm) was mixed in a BBO crystal with the Nd:YAG's third harmonic (355 nm). The resulting UV pulse (duration 7 ns, bandwidth 0.5 $cm^{-1}$), is tunable over the range 225–227 nm and separated in a set of four prisms. The pulses have a typical energy of 50 $\mu$J.

The output of a second Nd:YAG pumped dye (2) laser in the range 640–660 nm, is frequency-doubled in a KDP crystal resulting in a UV pulse with a bandwidth of 0.3 $cm^{-1}$ and tunable in the range 320–330 nm. This second UV pulse is used for the excitation from the $A\,^2\Sigma^+$ intermediate state to the Rydberg series converging toward the $NO^+\,^1\Sigma^+$ ionic ground state. The typical energy of the pulse is 150 $\mu$J. The field direction between the two metal plates in Fig. 2 is chosen such that the electrons are accelerated toward a microspheroid plate below and the total photoionization yield is detected as a function of excitation frequency. Simultaneously the laser intensity is monitored with a photodiode.

## IV. RESULTS AND DISCUSSION

Before employing the $1+1'$ excitation scheme we used $1+1$ resonantly enhanced multiphoton ionization (REMPI). The purpose of the measurement is to select appropriate rotational states for excitation to the Rydberg series and to check the influence of the static electric field on the position of the intermediate state. The rotational spectrum of the $A\,^2\Sigma^+$ intermediate state is well known[23,24] and we will not go into detail about this experiment. Resonant two-photon ionization via the $A\,^2\Sigma^+$ intermediate state ($v'=0$) is detected by focusing a UV pulse in a wavelength range of 223–230 nm and monitoring the total electron yield as a function of excitation frequency.

The selection of pure rotational states $N'$ from this spectrum is complicated by the presence of bandheads, i.e., higher rotational quanta overlap with lower ones and furthermore the *P*, *Q*, and *R* (corresponding to $\Delta J=-1,0,1$ respectively) branches overlap. In fact, the only rotational sequence that we found usable is the $P_{12}$ series on the very end of the low-energy side of the spectrum. This series does not have any overlap with other branches. It does show a bandhead structure but the relative population of higher rotational quanta compared to lower ones is minor at a low temperature. We estimate the temperature of the NO gas jet by fitting a Boltzmann distribution multiplied by the Höhn–London factors for a $\Sigma$-$\Pi$ transition to the $1+1$ REMPI spectrum. The temperature is about 130 K for all our experiments. At this temperature the selected $P_{12}(3/2)$ to $P_{12}(9/2)$ (where 3/2 and 9/2 is the total ground-state angular momentum *J*), corresponding to rotational angular momenta of $N'=0$, 1, 2, and 3, respectively, have overlap at the estimated 130 K with higher angular momenta with a maximum of 0.5%.

The $1+1$ REMPI spectrum was measured at various field strengths. In the range 0–2000 V/cm, no broadening of the lines was observed, only a slight shift on the order of the experimental bandwidth. This is not surprising in view of the small dipole moment of this state.

From now on the first UV pulse is set to excite one specific rotational state with decreased fluence. In this way we create some population in the intermediate state and suppress direct $1+1$ photoionization. The polarization of the laser is perpendicular to the electric field. In Fig. 3(a) a second UV pulse with a bandwidth of 0.3 $cm^{-1}$ excites the outer electron of the NO molecule from the $A\,^2\Sigma^+$ intermediate state ($N'=0, v'=0$; at 44 200.3 $cm^{-1}$) to Rydberg states converging to the $NO^+\,^1\Sigma^+$ ionic ground state. The solid lines show the photoelectron yield monitored as a function of excitation frequency in a static electric field of 1000 V/cm. The polarization of the excitation laser was either perpendicular or parallel with respect to the electric field. On the lower energy side there is no electron yield. Once the excitation energy is sufficient to excite Rydberg states above the saddlepoint of the potential, peaks start to appear in the ionization yield at a threshold of about 74 530 $cm^{-1}$ both for parallel and perpendicular excitation. Note that the photoionization spectrum of the NO molecule is, surprisingly, no more complex than the spectrum of a regular alkali atom.[1] Using this field strength and bandwidth of the excitation laser we are able to resolve the individual Stark states. Depicted above the spectra in Fig. 3(a) are the positions of the middle *k*-states of hydrogen of the $n=25$ and $n=26$ manifolds upon perpendicular excitation.

There is a distinctive difference in width of the Stark peaks depending on the polarization of the excitation laser. The width of the peaks at parallel excitation is around 1 $cm^{-1}$, corresponding to a lifetime of these states of about 15 ps. Perpendicular excitation, however, leads to longer lifetimes of the states and the width of these peaks is as narrow as 0.3 $cm^{-1}$. Since that is the bandwidth of the excitation laser, we can, from the experiment, only estimate a minimum lifetime of 50 ps for these states. The dependence of the lifetimes with the polarization may be understood in terms of the geometry of this system. There is both a direct and an indirect path for photoionization and it is the indirect path that gives the Stark resonances. An outgoing electron that is not ejected in the direction of the saddlepoint bounces off the wall of the potential and returns to the ionic core. However, after one radial oscillation the angular momentum has evolved toward higher *l* up to $l=n-1$. Higher angular momenta do not penetrate the ionic core and subsequently cannot scatter. Only after a full angular momentum oscillation the electron can scatter from the nonhydrogenic core into the direction of the saddlepoint resulting in autoionization. The broad peaks in the photoionization spectrum upon excitation

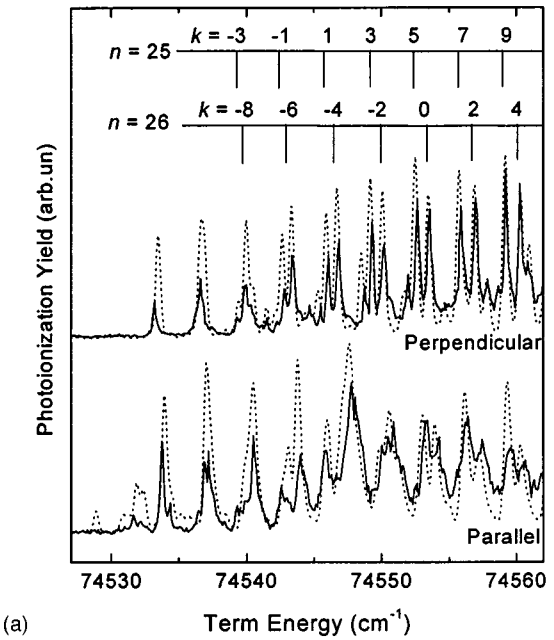


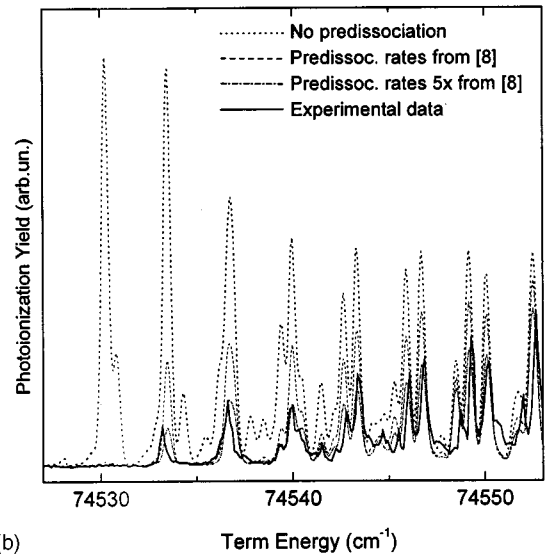


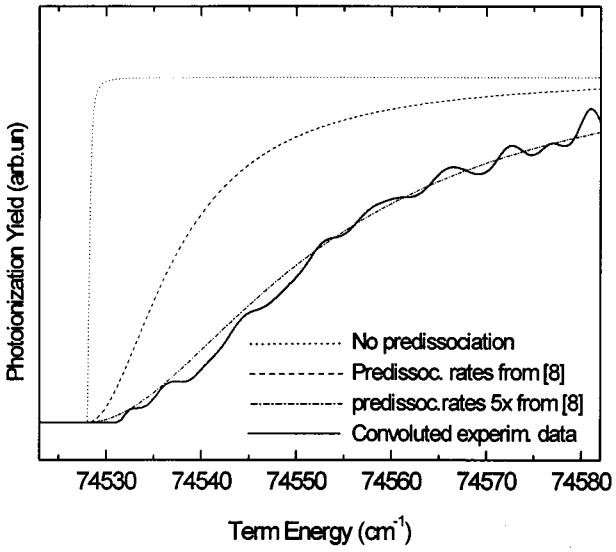


FIG. 3. (a) The total photoionization yield as a function of term energy via the $A\,^2\Sigma^+$ intermediate state with rotation $N'=0$. The laser polarization is either perpendicular or parallel with respect to the electric field of 1000 V/cm. The solid lines are the experimental data, the dotted lines are the calculated curves. The spectra are well reproduced by MQDT theory described in Sec. II B. Predissociation is included in the calculations with predissociation rates taken from Ref. 18. For comparison, the position of some $k$-states of the hydrogenic $n=25$ and $n=26$ manifolds upon perpendicular excitation are depicted. (b) Three calculations without (dotted line) and with predissociation (dashed line with rates taken from Ref. 8, dashed-dotted line five times faster) are compared to the experimental data (solid line) to illustrate the importance of including predissociation. All traces have perpendicular excitation. (c) Three calculations based on Eq. (13) without (dotted line) and with predissociation (dashed line with rates taken from Ref. 8, dashed-dotted line five times faster) are compared to the experimental data convoluted with a Gaussian of 3 $cm^{-1}$ (solid line). All traces have perpendicular excitation.

with parallel polarization indicate a single angular oscillation of the electron before autoionization, whereas perpendicular excitation leads to several recurrences of the electron before escaping.

An important observation in Fig. 3(a) is that the ionization peaks do not appear in a stepfunction-like manner but slowly increase in intensity. The number of peaks per unit energy increases with excitation energy converging on the high-energy side to a constant yield (the ionization potential in zero-field is at 74 721.7 $cm^{-1}$; Ref. 22). Calculation of the Rydberg series in an electric field by using the parameters of Table I and a convolution with a Gaussian having a width of 0.3 $cm^{-1}$ well simulates the observed photoionization spectra

TABLE II. Decay rates for state $n$: $\Gamma_0(l)/n^3$; taken from Ref. 8.

| | |
|---|---|
| $\Gamma_0(s)=500\ cm^{-1}$ | $\Gamma_0(f)=43\ cm^{-1}$ |
| $\Gamma_0(p)=1610\ cm^{-1}$ | $\Gamma_{eff}(l>3)=4\ cm^{-1}$ |
| $\Gamma_0(d)=1000\ cm^{-1}$ | |

far above ($>40$ $cm^{-1}$) the saddlepoint. Close to the saddlepoint, however, the calculation is only accurate concerning the position and width of the peaks. The discrepancy in intensity is diminished by including predissociation into the calculations. The dotted lines in Fig. 3(a) are calculations including the predissociation rates shown in Table II (taken from Ref. 8). In this energy region the rates are typically $10^9-10^{10}\ s^{-1}$.

To appreciate the effect of predissociation on the calculations of the photoionization yield in Fig. 3(b), three calculations are depicted, one without and two with different predissociation rates. All calculated traces are convoluted with a Gaussian having a width of 0.3 $cm^{-1}$. There is a dramatic decrease in intensity of the photoionization yield close to the saddlepoint upon including predissociation. Some peaks have completely vanished, making the photoionization threshold appear higher in energy. Furthermore, the stepfunction-like behavior of the photoelectron yield at threshold is lost and intensity only slowly increases with

higher excitation energy. Note that the agreement with the experimental results would improve even more by assuming a higher predissociation rate. The dash-dotted line in Fig. 3(b) includes a five times faster predissociation rate than suggested in Ref. 8 and is virtually indistinguishable from the experimental data.

That predissociation only decreases intensity in the region of about 40 $cm^{-1}$ above the saddlepoint lies in the fact that the escape angle of the Rydberg electron far above the saddlepoint is large and the electron autoionizes on subpicosecond time scales. Closer to the saddlepoint energy, however, the exit created by the electric field becomes narrow and the lifetime, hence the number of oscillations of the Rydberg electron, increases. After each angular oscillation the electron recurs to the core with low angular momentum $l$ and can couple to the predissociation channel. At the saddlepoint energy the predissociation is even dominant and the photoionization yield is completely quenched. Naturally the perpendicular excited states experience a larger influence of predissociation because of the longer lifetimes. It is useful to compare Eq. (13) derived in the theory section with the detected cross section convoluted with a Gaussian of 3 $cm^{-1}$ width [Fig. 3(c)]. The resolved Stark states are smoothed out and we can concentrate on the overall intensity behavior. As we already saw in Fig. 3(b), predissociation needs to be included and predissociation rates taken from Ref. 8 do not fit the experimental data very well. Five time faster rates are needed for a good fit. We have no explanation for the discrepancy except that the rates are extrapolated from higher $n(70-120)$ and lower fields ($<1$ V/cm).

Including predissociation in interpreting photoionization yield spectra of molecules in a static electric field is important to determine the saddlepoint energy. If one determines the saddlepoint energy by fitting the experimental spectra with a smoothed stepfunction, disregarding predissociation, one obtains a threshold that is too high in energy or, equivalently, the $\alpha$ from Eq. (2) would be too low. The photoionization yield measurements of nitric oxide in an electric field reported in Refs. 3 and 26 exhibit an apparent threshold that was higher in energy then expected. Instead of the theoretical $\alpha = 6.12\,cm^{-1}$, Ref. 3 reported 5.6 $cm^{-1}$ and Ref. 26 even 3.69 $cm^{-1}$! In Fig. 4 the photoionization yield spectra as a function of term energy are shown for various applied field strengths. The excitation is via the $N' = 0$ intermediate rotational state with polarization parallel to the electric field. Also shown is the saddlepoint energy as a function of electric field strength according to Eq. (2) with $\alpha = 6.12\,cm^{-1}$ (a) and $\alpha = 5.6\,cm^{-1}$ (b) taken from Ref. 3. By resolving the structure of Stark states and including predissociation in the calculation we find $\alpha = 6.12\,cm^{-1}$. By artificially cutting the high-frequency parts of the spectrum and fitting with a smoothed stepfunction like Refs. 3 and 26, we naturally obtain, when taking the midpoint of the rise, a lower $\alpha$ [in our case $\alpha = 5.7(1)\,cm^{-1}$].

In earlier studies on molecules in an electric field[5,27–30] Stark structure has been resolved. A saddlepoint, however, is not observed due to rotational or vibrational autoionization and we cannot compare the influence of predissociation to other molecules.

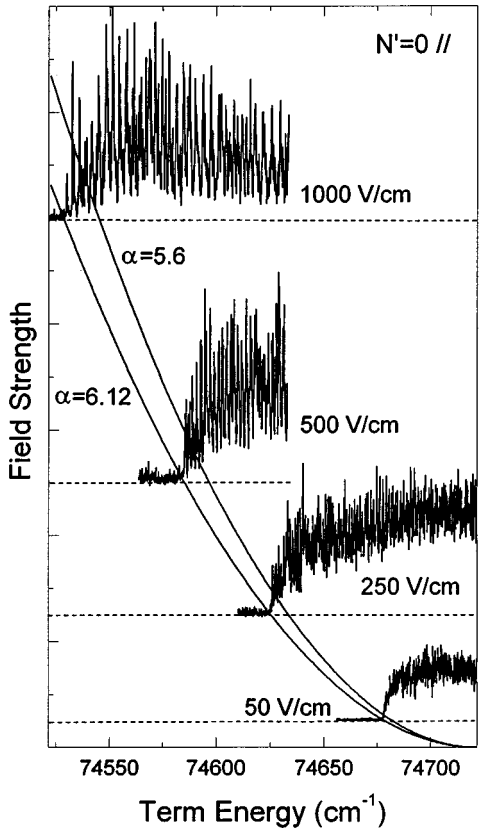


FIG. 4. The photoionization yield from $N' = 0$ as a function of term energy in electric fields of 1000, 500, 250, and 50 V/cm. The polarization of the excitation laser is parallel to the electric field. All structures seen are not noise but resolved Stark states. Plotted also is the position of the threshold in those fields with $\alpha = 6.12$ and $\alpha = 5.6$ as suggested by Ref. 3.

We now focus on the rotational dependence of the photoionization spectrum. As in Fig. 3(a), Fig. 5(a) shows the photoionization yield monitored as a function of excitation frequency of NO in an electric field of 1000 V/cm. The lowest trace in Fig. 5(a) is taken with excitation via the $A\,^2\Sigma^+$ intermediate rotational state $N' = 0$ (at 44 200.3 $cm^{-1}$). Three more traces are shown taken with excitation via the rotational states $N' = 1$, 2, and 3 (at 44 204.3, 44 212.2, and 44 224.1 $cm^{-1}$, respectively). For all traces, the laser polarization is perpendicular to the electric field. Starting from higher rotational states, the threshold is higher in energy. The theoretical saddlepoint energies are depicted with the dotted line. The increase of threshold energy corresponds to the increase of rotational energy $E_{rot}$ [Eq. (4)] with a rotational constant $B = 1.9842\,cm^{-1}$.[13] The only open channel for excitation lower than the saddlepoint energy via rotational states $N' > 0$ is excitation of a bound Rydberg state that decays by rotational autoionization into a lower $N'$ Rydberg series. The near absence of signal below the saddlepoint energies shows that the rotational autoionization is very weak; note that the competing predissociation channel sets an upper limit to the time during which rotational autoionization can take place.

Another argument for weak rotational coupling is shown in Fig. 5(b). Identical spectra are depicted as in Fig. 5(a) but now as a function of relative binding energy, i.e., energy compared to the ionization energy in zero-field of the se-

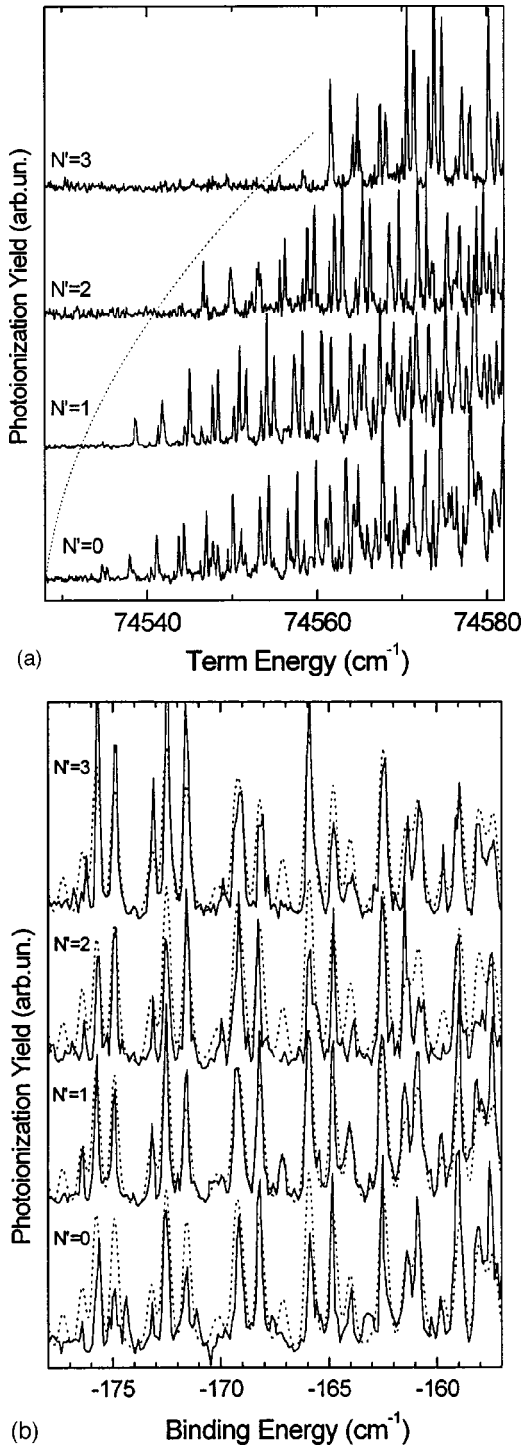


FIG. 5. (a) The total photoionization yield as a function of term energy. The four spectra are detected via the $A\,^2\Sigma^+$ intermediate state with rotations $N'=0$, 1, 2, and 3. The laser polarization is perpendicular with respect to the electric field of 1000 V/cm. For each higher rotation the apparent threshold is higher in excitation energy. The dotted line is the expected ionization threshold. (b) The solid lines are the same traces as for Fig. 5(a) but now as a function of relative binding energy, i.e., the term energy minus the ionization potential energy of the intermediate rotational states. The four spectra are detected with perpendicular excitation via the $A\,^2\Sigma^+$ intermediate state with rotations $N'=0$, 1, 2, and 3. Only a small energy range is shown to illustrate the similarity between the Rydberg series converging to the various rotational limits. The dotted lines are the calculated spectra.

lected intermediate rotational state. Only a small energy range is shown to illustrate the similarities between the Rydberg series converging to various rotational limits. The spectra are detected with perpendicular excitation via the $A\,^2\Sigma^+$ rotational states $N'=0$, 1, 2, and 3 (ionization energy $E_{(\mathrm{IP})}=74\,721.7$, $74\,725.7$, $74\,733.6$, and $74\,745.5$ $\mathrm{cm}^{-1}$, respectively). In this energy range the separate Stark states of overlapping $n$-manifolds can be distinguished. Comparison of the four traces reveals that the photoionization yield is very similar, independent of rotation. Only the intensity of the separate peaks differs somewhat. This suggests that the excitation occurs predominantly via the $Q$-branch ($N'-N^+=0$, as in Ref. 26) and only a weak rotational coupling changes the intensities of the peaks. In the case of nitric oxide, the dynamics of a complicated molecular ion and a Rydberg electron in a static electric field is considerably simpler than might be expected.

## V. CONCLUSIONS

We have investigated the photoionization of Rydberg electrons of the nitric oxide molecule. In a $1+1$ REMPI experiment we selected rotational states of the $A\,^2\Sigma^+$ intermediate state ($v'=0$) and monitored the dependence of a static electric field. Then the frequency of the first UV pulse was set to populate a specific rotational state and a second UV pulse was applied to excite to the Rydberg states. The excitation was done with polarization parallel or perpendicular to the electric field. The photoionization yield was monitored for autoionizing Rydberg states for NO in various electric fields and via different rotational states. The Stark structure in the spectra is fully understood and accurate simulations are achieved by quantum calculations based on MQDT. We observe that lifetimes of the Stark states are different upon different excitation polarization: parallel excitation leads to lifetimes of about 15 ps whereas perpendicular excitation leads to much longer lifetimes. An important observation is that predissociation quenches the photoionization yield close to the saddlepoint, which can lead to misinterpretation of photoionization threshold energy. A formula [Eq. (13)] for the average behavior of the photoionization cross section, including the effect of predissociation, gives insight into how the ionization signal is suppressed near threshold. The first peak on the low-energy side of the NO photoionization spectrum is therefore the onset of the Stark structure rather than the threshold of autoionization.

The photoionization spectra via various rotational states are compared and we observe that excitation occurs predominantly via the $Q$-branch. There is only weak rotational coupling leading to a lack of rotational autoionization and very similar photoionization spectra for the different rotational states of the core. In fact the spectra are very reminiscent of an alkali atom.

## ACKNOWLEDGMENTS

We gratefully thank M. J. J. Vrakking for fruitful discussions and V. Stravros and M. Noel (who participated thanks to a NATO travel grant CRG 920503) for assistance in the early stage of the experiment. The work described in this

paper is part of the research program of the FOM (Foundation for Fundamental Research on Matter) and was made possible by the financial support from the NWO (Netherlands Organization for the Advancement of Research). F.R. is also supported by the NSF. Computations were performed at the National Energy Research Supercomputer Center in Berkeley, CA.

[1] T. F. Gallagher, *Rydberg Atoms* (Cambridge University Press, Cambridge, 1994).
[2] E. W. Schlag, *ZEKE Spectroscopy* (Cambridge University Press, Cambridge, 1998).
[3] S. T. Pratt, J. L. Dehmer, and P. M. Dehmer, J. Chem. Phys. **90**, 2201 (1989).
[4] S. T. Pratt, J. Chem. Phys. **98**, 9241 (1993).
[5] C. R. Mohon, G. R. Janik, and T. F. Gallagher, Phys. Rev. A **41**, 3746 (1990).
[6] F. Merkt, H. H. Fielding, and T. P. Softley, Chem. Phys. Lett. **202**, 153 (1993).
[7] M. J. J. Vrakking, J. Chem. Phys. **102**, 8818 (1995).
[8] M. J. J. Vrakking, J. Chem. Phys. **105**, 7336 (1996).
[9] Y. Anezaki, T. Ebata, N. Mikami, and M. Ito, Chem. Phys. **97**, 153 (1985).
[10] M. Bixon and J. Jortner, J. Phys. Chem. **99**, 7466 (1995).
[11] M. Bixon and J. Jortner, J. Chem. Phys. **105**, 1363 (1996).
[12] F. Remacle and R. D. Levine, J. Chem. Phys. **105**, 4649 (1996).
[13] F. Remacle and M. J. J. Vrakking, J. Phys. Chem. A **102**, 9507 (1998).
[14] A. Giusti-Suzor and Ch. Jungen, J. Chem. Phys. **80**, 986 (1984).
[15] F. Fujii and N. Morita, J. Chem. Phys. **98**, 4581 (1993).
[16] A. Fujii and N. Morita, Laser Chem. **13**, 259 (1994).
[17] F. Robicheaux, C. Wesdorp, and L. D. Noordam, Phys. Rev. A (in press).
[18] D. A. Harmin, Phys. Rev. A **24**, 2491 (1981); **26**, 2656 (1982).
[19] D. J. Armstrong and C. H. Greene, Phys. Rev. A **50**, 4956 (1994).
[20] E. S. Chang and U. Fano, Phys. Rev. A **6**, 173 (1972).
[21] C. H. Greene and C. Jungen, Adv. At. Mol. Phys. **21**, 51 (1985).
[22] D. T. Biernacki and S. D. Colson, J. Chem. Phys. **89**, 2599 (1988).
[23] R. Engleman, Jr., and P. E. Rouse, J. Mol. Spectrosc. **37**, 240 (1971).
[24] W. G. Mallard, J. H. Miller, and K. C. Smith, J. Chem. Phys. **76**, 3483 (1982).
[25] S. N. Dixit, D. L. Lynch, V. McKoy, and W. M. Huo, Phys. Rev. A **32**, 1267 (1985).
[26] T. Ebata, Y. Anezaki, M. Fujii, N. Mikami, and M. Ito, J. Phys. Chem. **87**, 4773 (1983).
[27] W. L. Glab and K. Qin, J. Chem. Phys. **99**, 2345 (1993).
[28] Chr. Bordas, P. Brevet, M. Broyer, J. Chevaleyre, and P. Labastie, Europhys. Lett. **3**, 789 (1987).
[29] T. P. Softley, A. J. Hudson, and R. Watson, J. Chem. Phys. **106**, 1041 (1997).
[30] H. H. Fielding and T. P. Softley, Phys. Rev. A **49**, 969 (1994).